Boundary Layer Transition Prediction for RANS Flow Solvers

*E. A. Mayda** *and C. P. van Dam*†
Department of Mechanical & Aeronautical Engineering
University of California, Davis
One Shields Avenue
Davis, CA USA 95616

Abstract

A e^N database transition prediction model has been developed and implemented in a two-dimensional compressible RANS flow solver. The model is strongly coupled with the flow solver by way of laminar boundary layer properties extracted from the RANS solution. An amplification rate database was generated according to linear stability theory and allows for the efficient execution of the full e^N method. The new transition model was validated against a full stability code and produced comparable results while executing 1600 times faster. Subsonic and transonic RANS airfoil computations are presented to illustrate the capabilities of the model, the importance of transition prediction and compressibility effects on boundary layer stability.

1. Introduction

Accurate boundary layer transition prediction will play an important role in the design of future aerial vehicles. Ever increasing energy costs and environmental concerns underline the need for a leap forward in cruise performance for next-generation commercial airliners. Drag reduction will be a critical aspect of any new design. Aerodynamic improvements are possible if skin friction can be reduced by delaying the transition from a laminar to turbulent boundary layer, which is a design concept known as Natural Laminar Flow (NLF). Current efforts, such as Europe's TELFONA project,[1] seek to advance the technologies required to achieve natural laminar flow on large commercial aircraft. Development of accurate, robust transition-capable computational fluid dynamic codes will be essential to the design process. This paper will outline ongoing efforts to incorporate transition prediction methodologies into Reynolds-averaged Navier-Stokes (RANS) flow solvers. Focus is placed on a methodology that includes compressibility effects as well as flow unsteadiness. The former is important in the development of NLF aircraft operating at transonic conditions and the latter for capturing transition governed phenomena such as laminar separation bubbles.

In the following sections, a RANS-coupled boundary layer transition prediction method will be presented. First, background information regarding existing engineering methods for transition prediction will be covered. Next, the methods adopted for the present research effort will be outlined and validation cases will be shown. Finally, two-dimensional airfoil test cases will be presented and discussed.

2. Background

The topic of boundary layer stability and transition has been studied for over a century, and while much progress has been made, a theory of transition still does not exist. In the absence of a complete theory, engineers and scientists have worked to develop transition prediction methods which are useful for particular design and analysis applications. The predominant methods in use today employ either simplified or full versions of the semi-empirical e^N method pioneered by van Ingen[2] and Smith and Gamberoni.[3] The e^N approach is based upon boundary layer stability theory and allows for the prediction of transition by monitoring the amplification of small disturbances, called Tollmien-Schlichting (TS) waves, as they propagate downstream. In practice, the method tracks the growth of a constant frequency disturbance in

*Graduate Student Researcher
†Professor

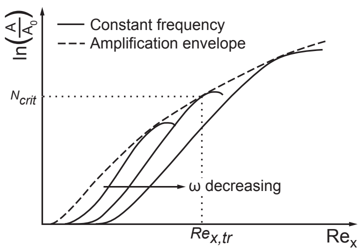

Figure 1: Constant frequency N-factor curves and the resulting envelope curve as calculated by the e^N method

either space or time according to growth rates determined via linear stability theory. Transition is predicted when the amplitude ratio, as calculated spatially in Eq. (1), reaches a critical limit, $e^{N_{\text{crit}}}$.

$$\frac{A}{A_0} = \exp\left[\int_{x_{\text{crit}}}^{x_{tr}} (-\alpha_i)\mathrm{d}x\right] = e^{N_{\text{crit}}} \tag{1}$$

Given a general distribution of boundary layer profiles, each of which has its own unique stability and growth rate characteristics, Eq. (1) is used to calculate the amplification curves shown in Fig. 1. Disturbances of each frequency will begin to grow once unstable Reynolds numbers are reached and will amplify until stability is regained (restablization causes the local maxima in the curves of Fig. 1). The disturbance amplitude curve that attains a value of N_{crit} at the lowest Re_x determines the transition location.

The empirical foundation for the e^N method lies with the choice for N_{crit}. By computing the N values at transition for a multitude of available experimental data, van Ingen[2] and Smith and Gamberoni[3] suggest that $N_{\text{crit}} \approx 9$. Based upon their spatial analysis, Jaffe et al.[4] found better correlation with experimental data for $N_{\text{crit}} \approx 10$, but they note that freestream turbulence and surface roughness act to decrease N_{crit} at transition. In 1977, Mack[5] proposed a correlation between freestream turbulence level, T, and critical N-factor:

$$N_{\text{crit}} \approx -8.43 - 2.4\ln(T), \tag{2}$$

which is valid for $0.0007 \leq T \leq 0.0298$. Through the use of Eq. (2), the e^N method is more flexible with respect to what type of flowfield and surface finish characteristics can be analyzed.

3. Methods

The approach taken for the present research effort is to closely couple an e^N method with a two-dimensional compressible RANS flow solver. The boundary layer stability calculation is conducted using a precompiled database of TS wave amplification rates which was generated with a compressible Orr-Sommerfeld solver. During run time, amplification rates are interpolated out of the database according to local integral boundary layer properties and edge values which are extracted from the current RANS flow solution. Transition locations are predicted using the e^N method described in Sec. 2 and are updated within the flow solver. For steady cases, the transition point movement is under-relaxed to maintain stability of the coupling method. When unsteady simulations are run, under-relaxed transition movement is conducted within the subiteration framework of the flow solver.

3.1 Flow Solver

The ARC2D flow solver developed by Pulliam and Steger[6] was chosen as the flow solver for the development phase of the present transition model, however, the model could be coupled with any similar code. ARC2D is a two-dimensional, compressible RANS flow solver. The code utilizes single structured, body-fitted meshes on which spatial derivatives are approximated with 2$^{\text{nd}}$-, 4$^{\text{th}}$- or 6$^{\text{th}}$-order centered finite differences. To aid in numerical stability, 2$^{\text{nd}}$- and 4$^{\text{th}}$-order artificial dissipation schemes in either scalar[7] or matrix[8] form are available. ARC2D contains several widely used turbulence models, but the Spalart-Allmaras model[9] is used exclusively in this paper.

3.2 Integral Boundary Layer Properties

The e^N database method described in the following section requires information regarding boundary layer development. In order to closely couple the transition model with the RANS flow solver, integral boundary layer properties and edge

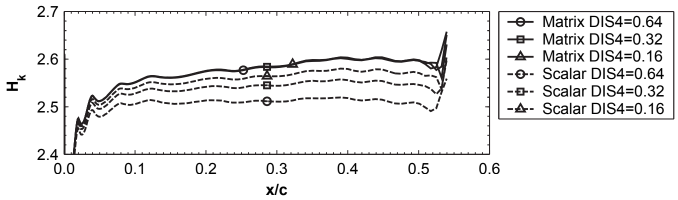

Figure 2: Kinematic shape factor variation caused by the choice of artificial dissipation scheme and fourth-order dissipation level (DIS4); curves represent the upper surface of the HSNLF(1)-0213 airfoil; $Re_c = 3.7\times10^6$, $M_\infty = 0.20$, $\alpha = 0°$, $(x/c)_{\text{trip,up}} = 0.55$ and $(x/c)_{\text{trip,low}} = 0.65$

quantities are extracted directly from the evolving RANS solution during run time. As mentioned in numerous papers (for example see Stock and Haase[10]), the boundary layer edge is difficult to locate in a RANS solution and if done improperly can lead to substantial errors in the calculation of integral parameters. In two-dimensional flows, the boundary layer edge velocity can be determined by integrating the vorticity distribution from the wall to the farfield along each normal gridline. The edge velocity, U_e, is taken as the wall-tangential velocity at the point where the ratio of the vorticity integral and its value at the farfield reaches a threshold value. The boundary layer thickness, δ, is then defined conventionally as the distance from the wall where $u(y) = 0.99U_e$.

After locating the boundary layer edge, the integral properties required for coupling can be calculated using a trapezoidal integration scheme. The compressible displacement thickness, δ^*, momentum thickness, θ, and shape factor, H, are defined as

$$\delta^* = \int_0^\delta \left(1 - \frac{\rho u}{\rho_e U_e}\right) \mathrm{d}y, \qquad \theta = \int_0^\delta \frac{\rho u}{\rho_e U_e}\left(1 - \frac{u}{U_e}\right) \mathrm{d}y, \qquad \text{and} \qquad H = \frac{\delta^*}{\theta}. \tag{3}$$

When taking compressibility into account, the value ranges for H defined in Eq. 3 vary substantially over the edge Mach number range of interest. To simplify the generation and storage of the amplification rate database, the kinematic version of shape factor, H_k, defined as

$$H_k = \frac{\delta_k^*}{\theta_k} \qquad \text{where} \qquad \delta_k^* = \int_0^\delta \left(1 - \frac{u}{U_e}\right) \mathrm{d}y \qquad \text{and} \qquad \theta_k = \int_0^\delta \frac{u}{U_e}\left(1 - \frac{u}{U_e}\right) \mathrm{d}y, \tag{4}$$

is used instead since its value range exhibits much less variation for $M_e \leq 1.5$.

The majority of previous attempts to couple transition methods with RANS solvers have found that calculating integral properties directly from the RANS solution produces inadequate results. This problem is likely caused by excessive dissipation which tends to make the laminar boundary layer behave in a turbulent-like fashion and manifests itself through incorrectly low shape factors. The use of an intermediate boundary layer code to reliably generate the needed data according to the RANS pressure distribution is the most common fix for this problem. Due to the desire for strong coupling and the need to eventually model unsteady flows, use of a boundary layer code is deemed impractical. While unwanted amounts of dissipation can be caused by exaggerated grid stretching in the boundary layer, choice of artificial dissipation scheme and fourth-order dissipation level has the most appreciable effect when an adequate grid is used. These effects are clearly shown in Fig. 2. In general, shape factor data quality increases as the dissipation level (DIS4) is decreased. However, the performance disparity between the scalar and matrix schemes is dramatic; the matrix scheme produces nearly identical shape factor distributions for all dissipation levels. For this reason, it is the only dissipation scheme used to generate the results in this paper.

3.3 e^N Database Method

Conducting a full e^N calculation using a compressible boundary layer stability code is precluded by the computational costs and non-robustness associated with a high fidelity analysis. In an effort to maintain the flexibility and accuracy of such an approach, the present method replaces the expensive stability calculation with an economical lookup operation that interpolates amplification rates from a database of stored values. The database was generated for families of attached, compressible, near-similarity boundary layer velocity profiles[11] and incompressible, separated profiles[12] using the Langley Stability and Transition Analysis Code[13] (LASTRAC) developed by Chang at NASA Langley Research Center.

Four database input variables are used to characterize the output generated by LASTRAC and allow coupling of the database method with the RANS solution. These quantities include edge Mach number, M_e, displacement thickness

Reynolds number, Re_{δ^*}, profile shape-shear parameter, A, and non-dimensional frequency, F, which are defined as

$$Re_{\delta^*} = \frac{\rho_e U_e \delta^*}{\mu_e}, \qquad A = \frac{1}{H_k}\left[\frac{\mathrm{d}\,(u/U_e)}{\mathrm{d}\,(y/\delta^*)}\right]_{\text{wall}}, \qquad \text{and} \qquad F = \frac{2\pi\mu_e}{\rho_e U_e^2} f, \tag{5}$$

where f is the dimensional frequency in Hz. For $M_e \geq 0.7$ oblique TS wave angles can be important, but the spanwise wave number, β, is not included as an input variable. Instead, amplification rates were maximized with respect to β during database generation.

When a transition prediction call is made from within the flow solver, boundary layer properties are calculated from the current RANS solution as described in Sec. 3.2. A range of frequencies for tracking with the e^N method is then established based upon the laminar boundary layer thickness. For each frequency, an N-factor curve is calculated using a trapezoidal approximation to Eq. 1. The amplification rates, $-\alpha_i$, required for this step are retrieved from the database using local n^{th}-order Lagrangian interpolation.[14] An envelope curve is formed by taking the maximum N value attained by any mode in the frequency range at each streamwise location. Transition is predicted to occur when the envelope curve first reaches the specified threshold, N_{crit}. Under-relaxation is used to update the transition locations used in the flow solver so that any position oscillations are damped. Finally, flow solver iteration resumes until the next transition call is made, and the process continues until a converged solution is attained.

3.4 Validation Cases

Flat plate and airfoil validation cases are presented to test the assumptions made during the generation of the database and to test accuracy of the interpolation methods. A compressible boundary layer code[15] was used to generate candidate flow solutions for both LASTRAC and the present e^N database method to analyze. Excellent agreement between the full stability analysis and the database treatment is achieved for the $M_\infty = 0.01$ and 0.50 cases as shown in Fig. 3. At the two higher Mach numbers ($M_\infty = 1.0$ and 1.5), slight disagreement is apparent for the lower frequency modes. This is caused by interpolation error and could be improved by including more velocity profiles (more shape factors, H_k) in the database at the expense of larger database size. Agreement is excellent for the higher frequencies, which would not have been possible without accounting for the presence of oblique modes ($\beta \neq 0$). Figure 3 also illustrates the stabilizing effect compressibility has on the flat plate flow. Amplification rates are reduced as the Mach number is increased, and the N-factor envelope curves reach critical values farther downstream. For example, an N value of 9.0 is attained at $Re_x = 3.22\times10^6,\ 3.96\times10^6,\ 7.39\times10^6,$ and 11.84×10^6 for $M_\infty = 0.01,\ 0.50,\ 1.0$ and 1.5, respectively.

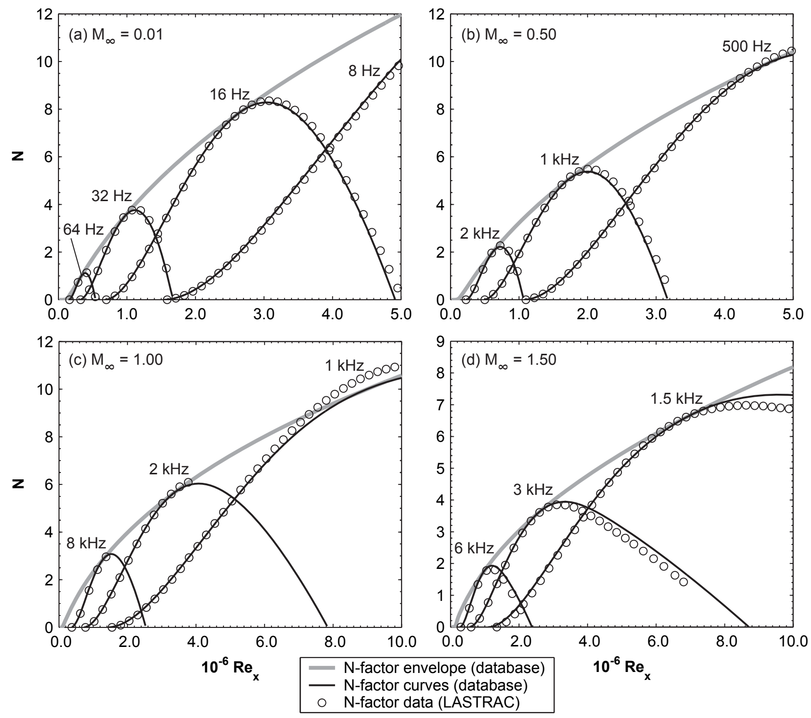

Figure 3: N-factor distributions for flat plate flow comparing results from LASTRAC and the present e^N database method for various Mach numbers: (a) $M_\infty = 0.01$, (b) $M_\infty = 0.50$, (c) $M_\infty = 1.00$ and (d) $M_\infty = 1.50$ ($T_\infty = 288\text{K}$)

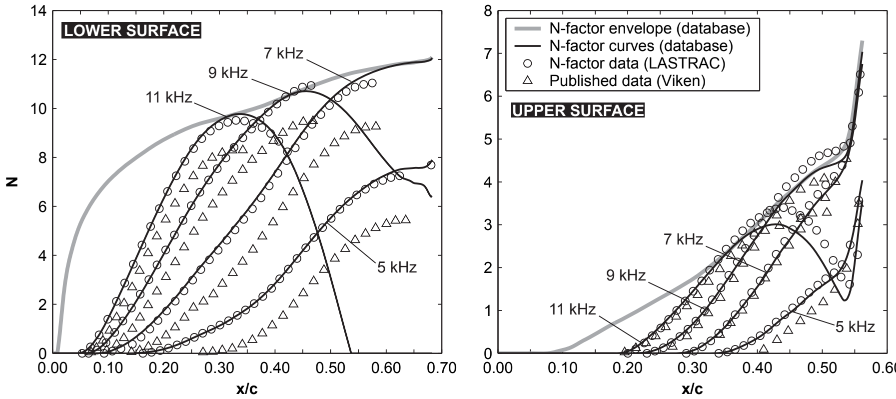

Figure 4: N-factor distributions for the HSNLF(1)-0313 airfoil comparing results from LASTRAC, the present e^N database method and published computational data from Viken and Wagner;[16] $Re_c = 40 \times 10^6$, $M_\infty = 0.70$, $T_\infty = 238.64$ K, $C_\ell = 0.26$, $c = 1.2192$ m

A transonic airfoil test case was chosen to validate the database method for varying shape factor conditions. Published computational results are available for the HSNLF(1)-0313 airfoil which was designed and analyzed by Viken and Wagner[16] using inviscid pressure distributions, a boundary layer solver[15] and the COSAL[17] stability code. The same approach was taken to produce the candidate flow solutions needed to compare LASTRAC and the database method. As with the flat plate cases, very good agreement between the two codes is exhibited in Fig. 4. Additionally, the upper surface results also compare very well with Viken and Wagner's data even though very different tools were employed. Published data for the lower surface generally lie below those calculated by LASTRAC or with the database method. N-factor curves generated with LASTRAC while neglecting oblique modes, however, were found to agree very well with Viken and Wagner's results (not shown in Fig. 4 for clarity).

3.5 Relative Performance of Stability Analysis Methods

While the database model does show small deviations from the LASTRAC results in the preceding section, its general use proved to be much more robust and computationally efficient than LASTRAC. A timing study of the two codes reveals that the database approach is approximately 1600 times faster than the full stability analysis. This estimated speedup is highly conservative since best-case scenarios were used to evaluate LASTRAC's execution time. For example, the LASTRAC cases did not include any costly oblique mode analyses which do not incur any performance penalty for the database method.

4. Results and Discussion

In the following sections, subsonic and transonic RANS results will be presented for the HSNLF(1)-213 and NACA0012 airfoils. The HSNLF(1)-0213 is a high-speed natural laminar flow (HSNLF) airfoil designed for use on a prototype business jet.[18] The design exploits stabilizing compressibility effects and achieves long runs of laminar flow for chord Reynolds numbers in excess of 11×10^6. The NACA0012, a turbulent airfoil by design, also demonstrates compressibility's influence on boundary layer stability and transition.

4.1 Grid Generation

All grids used for the RANS calculations were generated with the Chimera Grid Tools[19] software suite. C-meshes were generated for both the HSNLF(1)-0213 and NACA0012 geometries. Surface spacing ($\Delta s/c$) was 0.001 at the leading and trailing edges, maximum surface spacing was limited to 0.01, and the maximum geometric stretching ratio was 1.2. Local surface refinement of 0.005 for $0.6 \leq x/c \leq 0.8$ was used on the HSNLF(1)-0213 mesh to better resolve laminar separation bubbles which were likely to occur. Wake cuts extended from trailing edge to a farfield distance of $50c$ using a maximum stretching ratio of 1.2. The flow domain meshes were grown from the airfoil surface using a hyperbolic grid generator, and initial wall spacing was chosen to ensure that $y^+ \leq 1$ for the chord Reynolds numbers being studied. Approximately 125 points are used within $0.02c$ of the wall to adequately resolve the boundary layer velocity profiles. Elliptic smoothing was performed on the wake region of the grid to expand the excessively fine spacing at the wake

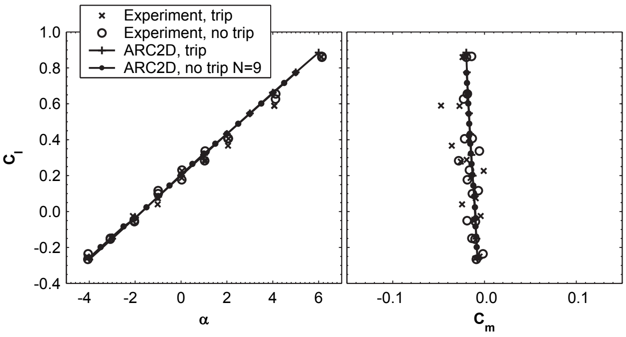

Figure 5: HSNLF(1)-0213 lift and pitching moment coefficients; experimental data from Sewall et al.;[18] $(x/c)_{\text{trip}}$ = 0.05, $Re_c = 3.7 \times 10^6$, $M_\infty = 0.2$

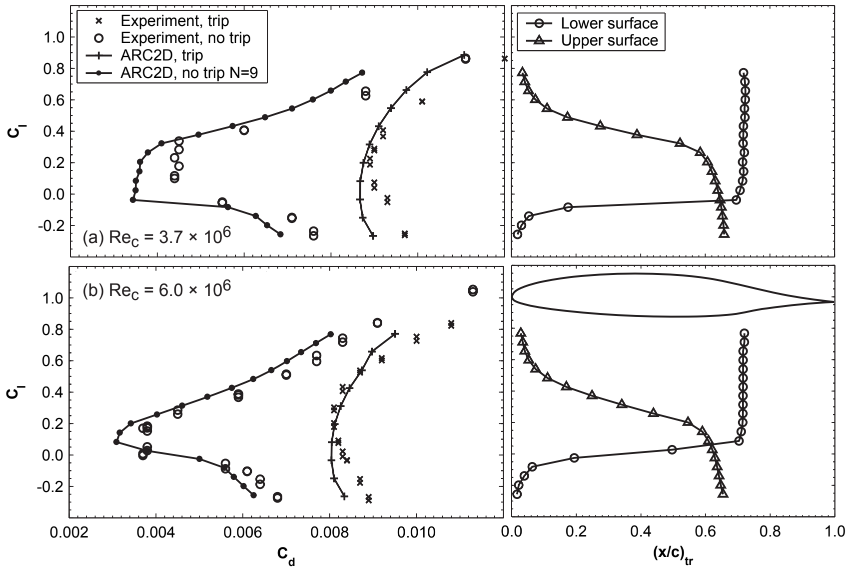

Figure 6: HSNLF(1)-0213 drag polars and transition locations; experimental data from Sewall et al.;[18] $(x/c)_{\text{trip}} = 0.05$ (a) $Re_c = 3.7 \times 10^6$, $M_\infty = 0.20$, (b) $Re_c = 6.0 \times 10^6$, $M_\infty = 0.14$

cut caused by the y^+ requirement. Grid dimensions for the HSNLF(1)-0213 and NACA0012 airfoils are 557 × 176 and 501 × 184, respectively. A grid refinement study following the method of Zingg[20] was conducted on both grids by halving the number of points in each curvilinear direction to create coarse versions of the meshes. Fully turbulent cases, representative of those in the following sections, were run for all grids, and truncation error was found to be less than ±0.544% for C_ℓ and C_d at transonic conditions and less than ±0.3% at subsonic speeds. Free transition grid convergence cases were not possible due to the coarseness of the meshes near the wall.

4.2 Subsonic Results

The HSNLF(1)-0213 airfoil was analyzed at two flow conditions ($Re_c = 3.7 \times 10^6$, $M_\infty = 0.20$ and $Re_c = 6.0 \times 10^6$, $M_\infty = 0.14$) for which experimental data[18] are available for comparison. Lift and quarter-chord pitching moment coefficient results are plotted in Fig. 5 for the $Re_c = 3.7 \times 10^6$ case. Very good agreement is shown over the angle of attack range considered, and the higher Re_c case (not shown) exhibits the same behavior. While transition has little impact on the lift and moment performance of thin airfoils at low angles of attack, it has a substantial effect upon the measured and predicted drag as shown in Fig. 6. RANS drag coefficient values with the boundary layer tripped at $x/c = 0.05$ compare well with the corresponding experimental data at both Reynolds numbers and suggest that the grid generation and turbulence modeling approaches are sufficient for the problem.

Transitional cases, designated "no trip" in Fig. 6, where analyzed according to an N_{crit} of 9.0. This corresponds to a freestream turbulence intensity of 0.07% (see Eq. 2) which conservatively approximates the conditions in the Langley Low Turbulence Pressure Tunnel.[21] Good correlation between measured and calculated drag is demonstrated

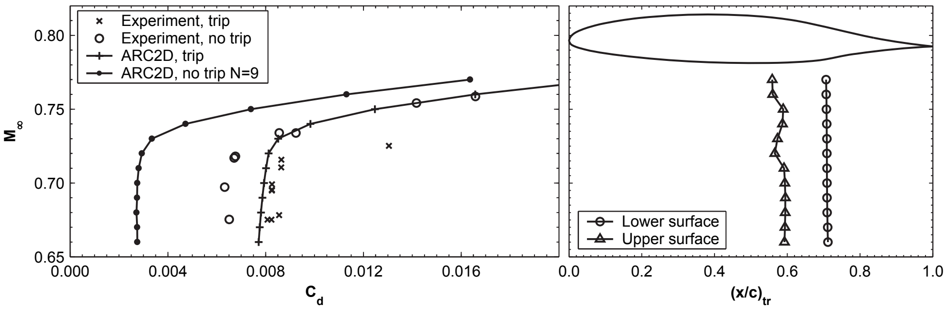

Figure 7: HSNLF(1)-0213 drag coefficient and transition locations versus Mach number; uncorrected experimental data from Sewall et al.;[18] $(x/c)_{\text{trip}} = 0.05$, $C_\ell = 0.26$, $Re_c = 11 \times 10^6$, $T_\infty = 288$K (○ Experiment, no trip: $Re_c = 4 \times 10^6$)

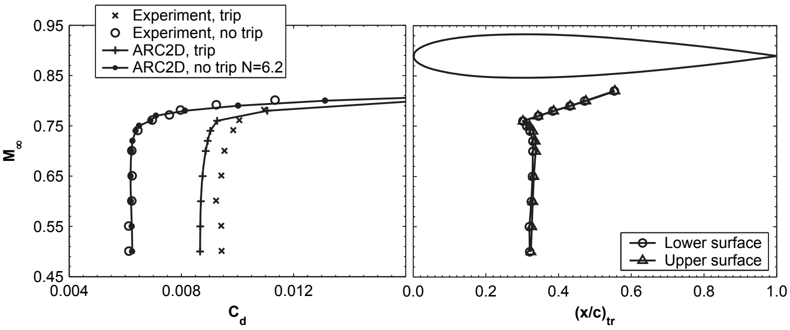

Figure 8: NACA0012 drag coefficient and transition locations versus Mach number; uncorrected experimental data from Harris;[22] $(x/c)_{\text{trip}} = 0.05$, $\alpha = 0°$, $Re_c = 3 \times 10^6$, $T_\infty = 288$K

although the computed values are roughly 8 drag counts low. Sensitivity of the calculated drag to choice of N_{crit} was investigated but was found not to improve agreement. The drag bucket present in the experimental data is also predicted by the RANS calculations due to use of the e^N database model. The fore-aft movement of the upper and lower surface transition locations caused by changing lift conditions gives rise to the drag bucket when both surfaces experience extended runs of laminar flow. This is best illustrated by the transition location plots in Fig. 6. When comparing Fig. 6(a) and 6(b), it is demonstrated that increasing the chord Reynolds number causes the transition locations to move forward earlier which results in reduced drag bucket width and reduced minimum drag. One final topic worth noting is that the lower surface transition location is nearly constant for $C_\ell \gtrsim 0.0$. This behavior is indicative of a laminar-turbulent separation bubble and is a common cause of transition for natural laminar flow designs.

4.3 Transonic Results

In addition to the validation case shown in Fig. 4, two transonic RANS airfoil cases are given which demonstrate the capabilities of the e^N database and the importance of including transition modeling in future computational analyses. The first case examines the performance of the HSNLF(1)-0213 airfoil at a cruise lift coefficient of 0.26 over a freestream Mach number range of 0.66 to 0.77. Figure 7 compares the RANS results with the experimental data,[18] which are not corrected for wall effects. Favorable agreement is achieved for $M_\infty \lesssim 0.72$ with tripped boundary layer conditions. Non-tripped experimental data for $Re_c = 4 \times 10^6$ are also available and are plotted in Fig. 7. Unfortunately, poor flow quality in the 6- by 8-Inch Transonic Tunnel greatly reduces the data's value for comparison purposes. Nonetheless, it is useful to investigate the theoretical performance of the HSNLF concept by considering natural boundary layer transition. At normal cruise flight conditions, flow quality can be characterized by $N_{\text{crit}} \geq 9.0$ so a conservative value of 9.0 was used in the performed RANS calculations. The computed free transition drag performance, plotted in Fig. 7, shows that significant improvement can be realized as compared to fully turbulent operation. Drag coefficients below 0.0030 are achieved for $M_\infty \leq 0.72$ which represents a viscous drag reduction of at least 50 counts. For these cases, laminar flow is maintained up to $0.59c$ and $0.71c$ on the upper and lower surfaces, respectively.

The capability to predict transition at transonic conditions has implications for the analysis of non-NLF designs in addition to the HSNLF results just presented. Experimental results[22] for the NACA0012 airfoil, plotted in Fig. 8, show that the drag coefficient can differ by up to 33 counts when tested with and without boundary layer trips. RANS computations mimicking the tunnel tests exhibit similar trends when using $N_{\mathrm{crit}} = 6.2$ to model the reported tunnel flow quality.[23] A drag reduction of $\Delta C_d \approx 0.0025$ is accomplished by delaying transition to $0.33c$ for $M_\infty \leq 0.72$. At slightly higher Mach numbers, $0.72 < M_\infty < 0.76$, the transition location moves forward due to a steepening of the pressure recovery caused by increasing amounts of supersonic flow and reduced minimum pressure coefficient. Finally, for $M_\infty \geq 0.76$ compressibility effects become strong enough to modify the pressure distribution, stabilize the boundary layer and move the transition locations aft. Transition eventually occurs at the shock due to the highly adverse pressure gradient and its effect on the boundary layer.

5. Conclusion

Accurate prediction of boundary layer transition at subsonic and transonic speeds will be vital to the design of future air vehicles. For this reason, a full e^N database transition prediction model for Tollmien-Schlichting type disturbances was developed and implemented in the two-dimensional compressible RANS flow solver, ARC2D. The new model and solver are strongly coupled via use of laminar boundary layer properties derived directly from the evolving RANS solution. Amplification rates required by the e^N method are stored in a database and are retrieved using local Lagrangian interpolation. The database was generated for a family of compressible near-similarity velocity profiles using the LASTRAC stability code.

Flat plate and airfoil validation cases were presented which demonstrate the database model's capability to characterize the same analyses performed by LASTRAC. The database method was found to be more robust and at least 1600 times faster than the full stability analysis. Two-dimensional subsonic and transonic airfoil RANS flow calculations were shown to compare very well with available experimental data for both free transition and tripped conditions. Predicted movement of the transition locations gives rise to the drag bucket phenomenon common to natural laminar flow designs and illustrates the need to incorporate transition modeling in RANS flow solvers. Finally, transonic airfoil results show that boundary layer transition also plays a vital role at higher Mach numbers. Boundary layer-stabilizing compressibility effects make it possible to achieve extended runs of laminar flow at relatively high chord Reynolds numbers for high-speed natural laminar flow designs. Performance benefits are also realized for conventional turbulent airfoil designs when free transition conditions are considered.

Acknowledgements

The authors would like to thank Roger Strawn of the U.S. Army Aeroflightdynamics Directorate for support of this project through Interchange NNA06CB77A. The guidance provided by Chau Chang of NASA Langley Research Center proved invaluable during the e^N database development using the LASTRAC code. Finally, the continued support of the ARC2D flow solver by Thomas Pulliam of NASA Ames Research Center is greatly appreciated.

References

[1] Sawyers, D., "An Overview of the TELFONA Project," *Paper 663, European Conference on Computational Fluid Dynamics (ECCOMAS CFD)*, 2006.

[2] van Ingen, J. L., "A Suggested Semi-Empirical Method for the Calculation of the Boundary Layer Transition Region," Report VTH-74, Dept. of Aeronautics and Engineering, Institute of Technology, Delft, The Netherlands, 1956.

[3] Smith, A. M. O. and Gamberoni, N., "Transition, Pressure Gradient and Stability Theory," Report No. ES 26388, Douglas Aircraft Company, Long Beach, CA, August 1956.

[4] Jaffe, N. A., Okamura, T. T., and Smith, A. M. O., "Determination of Spatial Amplification Factors and Their Application to Predicting Transition," *AIAA Journal*, Vol. 8, No. 2, February 1970, pp. 301–308.

[5] Mack, L. M., "Transition Prediction and Linear Stability Theory," In AGARD CP-244, NATO, Paris, 1977, pp. 1-1 to 1-22.

[6] Pulliam, T. H., "Efficient Solution Methods for the Navier-Stokes Equations," *Lecture Notes for the von Kármán Institute For Fluid Dynamics Lecture Series: Numerical Techniques for Viscous Flow Computation In Turbomachinery Bladings*, von Kármán Institute, Rhode-St-Genèse, Belgium, 1985.

[7] Jameson, A., Schmidt, W., and Turkel, E., "Numerical Solutions of the Euler Equations by Finite Volume Methods Using Runge-Kutta Time-Stepping Schemes," *AIAA Paper 81-1259, 14th AIAA Fluid and Plasma Dynamics Conference*, Palo Alto, California, 1981.

[8] Turkel, E., "Improving the Accuracy of Central Difference Schemes," NASA CR 181712, September 1988.

[9] Spalart, P. and Allmaras, S., "A One-Equation Turbulence Model for Aerodynamic Flows," *AIAA Paper 92-0439, 30th AIAA Aerospace Sciences Meeting and Exhibit*, Reno, NV, January 1992.

[10] Stock, H. W. and Haase, W., "Feasibility Study of e^N Transition Prediction in Navier-Stokes Methods for Airfoils," *AIAA Journal*, Vol. 37, No. 10, October 1999, pp. 1187–1196.

[11] Horton, H. P., "Near-Similarity Approximation for Compressible, Laminar Boundary Layers on Adiabatic Walls," *Proceedings of the Institution of Mechanical Engineers – Part G – Journal of Aerospace Engineering*, Vol. 211, No. 5, 1997, pp. 285–294.

[12] Dini, P., Selig, M. S., and Maughmer, M. D., "Simplified Linear Stability Transition Prediction Method for Separated Boundary Layers," *AIAA Journal*, Vol. 30, No. 8, August 1992, pp. 1953–1961.

[13] Chang, C.-L., "Langley Stability and Transition Analysis Code (LASTRAC) Version 1.2 User Manual," NASA TM 2004-213233, June 2004.

[14] Press, W. H., Teukolsky, S. A., Vetterling, W. T., and Flannery, B. P., *Numerical Recipes in Fortran 77: The Art of Scientific Computing*, Cambridge University Press, 2nd ed., 1992.

[15] Harris, J. E. and Blanchard, D. K., "Computer Program for Solving Laminar, Transitional, or Turbulent Compressible Boundary-Layer Equations for Two-Dimensional and Axisymmetric Flow," NASA TM 83207, February 1982.

[16] Viken, J. and Wagner, R. D., "Design Limits of Compressible NLF Airfoils," *AIAA Paper 91-0067,* 29th *Aerospace Sciences Meeting*, Reno, NV, January 1991.

[17] Malik, M. R., "COSAL - A Black-Box Compressible Stability Analysis Code for Transition Prediction in Thee-Dimensional Boundary Layers," NASA CR 165925, May 1982.

[18] Sewall, W. G., Mcghee, R. J., Viken, J. K., Waggoner, E. G., Walker, B. S., and Millard, B. F., "Wind Tunnel Results for a High-Speed, Natural Laminar-Flow Airfoil Designed for General Aviation Aircraft," NASA TM 87602, November 1985.

[19] Chan, W. M., Rogers, S. E., Nash, S. M., Buning, P. G., and Meakin, R. L., *User's Manual for Chimera Grid Tools, Version 1.9*, October 2004, available as of May 2007 at http://people.nas.nasa.gov/˜wchan/cgt/doc/man.html.

[20] Zingg, D. W., "Grid Studies for Thin-Layer Navier-Stokes Computations of Airfoil Flowfields," *AIAA Journal*, Vol. 30, No. 10, 1992, pp. 2561–2564.

[21] McGhee, R. J., Beasley, W. D., and Foster, J. M., "Recent Modifications and Calibration of the Langley Low-Turbulence Pressure Tunnel," NASA TP 2328, January 1984.

[22] Harris, C. D., "Two-dimensional Aerodynamic Characteristics of the NACA 0012 Airfoil in the Langley 8 Foot Transonic Pressure Tunnel," NASA TM 81927, April 1981.

[23] Harvey, W. D., Stainback, P. C., and Owen, F. K., "Evaluation of Flow Quality in Two Large NASA Wind Tunnels at Transonic Speeds," NASA TP 1737, December 1980.

This page has been purposedly left blank